Gen Relativ Gravit (2012) 44:1857–1879
DOI 10.1007/s10714-012-1368-x

RESEARCH ARTICLE

Schwarzschild black hole surrounded by quintessence: null geodesics

Sharmanthie Fernando

Received: 13 February 2012 / Accepted: 19 April 2012 / Published online: 1 May 2012

Abstract We have studied the null geodesics of the Schwarzschild black hole surrounded by quintessence matter. Quintessence matter is a candidate for dark energy. Here, we have done a detailed analysis of the geodesics and exact solutions are presented in terms of Jacobi-elliptic integrals for all possible energy and angular momentum of the photons. The circular orbits of the photons are studied in detail. As an application of the null geodesics, the angle of deflection of the photons are computed.

Keywords Static · Black holes · Geodesics · Dark energy · Quintessence

1 Introduction

It is well known that we live in a universe undergoing a period of accelerating expansion. This indicates the presence of mysterious form of repulsive gravity called dark energy. There are several observations that support dark energy. One is the studies of type Ia supernova [1–3]. The other is the observations related to the cosmic microwave background (CMB) [4] and large scale structure (LSS) [5,6].

The nature of dark energy is yet to be understood. There are several cosmological models proposed in which the dominant component of the energy density has negative pressure. One of them is the cosmological constant Λ which corresponds to the case of dark energy with a state parameter $\omega_q = -1$. However, there is a key problem that is yet to be understood about the cosmological constant from the point

S. Fernando (✉)
Department of Physics and Geology, Northern Kentucky University,
Highland Heights, KY 41099, USA
e-mail: fernando@nku.edu

of view of fundamental physics. Its observed value is too small which is also called the fine-tuning problem [8].

There are alternative models that are proposed as candidates for dark energy. Most of these models are based on a scalar field. Such scalar field models include but not limited to, quintessence [9], chameleon fields [10], K-essence [11], tachyon field [12], phantom dark energy [13] and dilaton dark energy [14]. For a detailed review of various models of dark energy see [7].

Given the fact that dark energy contains about 70 % of the universe and black holes are also accepted as part of our universe, studies of black holes surrounded by dark energy takes an important place in research. In this paper, we study the Schwarzschild black hole surrounded by quintessence matter. Quintessence is described as a scalar field coupled to gravity with a potential that decreases as the field increases [9,7]. Kiselev [15] derived black hole solutions surrounded by quintessence matter which has the state parameter in the range, $-1 < \omega_q < -\frac{1}{3}$. In this paper, we will focus on the solution derived by Kiselev.

There are several works done on the black hole derived by Kiselev in the literature. The quasinormal modes of the black holes has been computed extensively. The quasinormal modes of the Schwarzschild black hole surrounded by the quintessence matter has been computed in [16–19]. The quasinormal modes of the Reissner-Nordstrom black hole surrounded by the quintessence matter has been presented in [20]. Hawking radiation of d-dimensional extension of the Kiselev black hole has been studied by Chen et. al. in [21].

The main objective of this paper is to study the geodesic structure of massless particles of the Schwarzschild black hole surrounded by quintessence matter. The motion of particles around black holes has been studied extensively in the literature for all types of black holes. Due to the large volume of papers related to this subject, we will avoid referring the papers here. Motion of particles around a black hole is one way to understand the gravitational field around a black hole. Given the fact that dark energy is one of the most important issues need to be resolved in physics, the studies of particles around a black hole immersed in dark energy take an important place.

The paper is presented as follows: In Sect. 2 the black hole solutions surrounded by quintessence matter is introduced. In Sect. 3 the general formalism of the geodesics are given. In Sect. 4, the radial geodesics are discussed. In Sect. 5, the geodesics with angular momentum are discussed. In Sect. 6, the geodesics are analyzed with a new parameter. In Sect. 7, the applications of the null geodesics are given. Finally, the conclusion is given in Sect. 8.

2 Schwarzschild black hole surrounded with quintessential matter

In this section we will give an introduction to the Schwarzschild black hole solutions surrounded by quintessential matter obtained by Kiselev [15]. The geometry of such a black hole has the metric of the form,

$$ds^2 = -g(r)dt^2 + g(r)^{-1}dr^2 + r^2(d\theta^2 + \sin^2\theta d\phi^2) \tag{1}$$

where,

$$g(r) = 1 - \frac{2M}{r} - \frac{c}{r^{3w_q+1}} \tag{2}$$

Here, M is the mass of the black hole and w_q is the state parameter of the quintessence mater. c is a normalization factor. The parameter w_q has the range,

$$-1 < w_q < -\frac{1}{3} \tag{3}$$

The equation of state for the quintessence mater is given by,

$$p_q = w_q \rho_q \tag{4}$$

and

$$\rho_q = -\frac{c}{2}\frac{3w_q}{r^{3(1+w_q)}} \tag{5}$$

Here p_q is pressure and ρ_q is the energy density. As described in [15], to cause acceleration, the pressure of the quintessence matter p_q has to be negative. The mater energy density ρ_q is positive. Hence the parameter $c > 0$ for negative w_q. For more details on the derivation of the solutions and the basis to choose the parameters as given, reader is referred to the paper by Kiselev [15].

One can observe that for $w_q = -1$, the function $g(r)$ for the metric reduces to

$$g(r) = 1 - \frac{2M}{r} - cr^2 \tag{6}$$

which is the Schwarzschild-de-Sitter black hole space-time.

In this paper, we will focus on the special case of $w_q = -\frac{2}{3}$. Then,

$$g(r) = 1 - \frac{2M}{r} - cr \tag{7}$$

For $8Mc < 1$, the metric with the above $g(r)$ given in Eq. (7) has two horizons as,

$$r_{\text{in}} = \frac{1 - \sqrt{1 - 8Mc}}{2c} \tag{8}$$

$$r_{\text{out}} = \frac{1 + \sqrt{1 - 8Mc}}{2c} \tag{9}$$

The inner horizon r_{in} is like the Schwarzschild black hole horizon. The outer horizon r_{out} is a cosmological horizon similar to what is observed in the Schwarzschild-de-Sitter black hole. Notice for small c, $r_{\text{out}} \approx \frac{1}{c}$ which is similar to $r_{\text{out}} \approx \sqrt{\frac{3}{\Lambda}}$ for small Λ in the Schwarzschild-de-Sitter case. There is a static region between the two horizons.

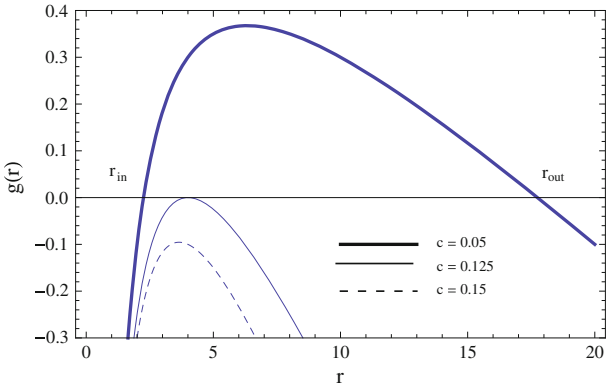

Fig. 1 The graph shows the relation of $g(r)$ with r for various values of the parameter c. Here, $M = 1$

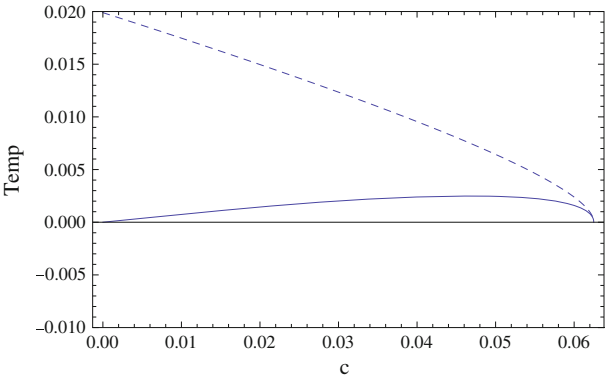

Fig. 2 The graph shows the relation of the temperature with c for both horizons. The *dashed curve* is for the inner horizon while the *thick curve* is for the outer horizon. Here, $M = 2$

Hence, in considering the motion of photons, we will focus on the region between the two horizons.

If $8Mc = 1$, the space-time has a degenerate solution at $r = \frac{1}{2c}$. For $8Mc > 1$, there are no horizons. All three situations are represented in Fig. 1.

The Hawking temperature for this black hole is,

$$T_{r_{\text{in}},r_{\text{out}}} = \frac{1}{4\pi}\left|\frac{dg_{tt}}{dr}\right|_{r=r_{\text{in,out}}} \tag{10}$$

which leads to,

$$T_{r_{\text{in}},r_{\text{out}}} = \frac{1}{4\pi}\left|\frac{2M}{r^2_{\text{in,out}}} - c\right| \tag{11}$$

The temperature for both horizons are plotted in Fig. 2. The temperature of the outer horizon is smaller than the inner horizon.

3 Geodesics of the black hole

We will derive the geodesic equations for neutral particles around the quintessence black hole. We will follow the same approach given in the well known book by Chandrasekhar [22]. The equations governing the geodesics in the space-time given in Sect. 2 can be derived from the Lagrangian equation,

$$\mathcal{L} = -\frac{1}{2}\left(-g(r)\left(\frac{dt}{d\tau}\right)^2 + \frac{1}{g(r)}\left(\frac{dr}{d\tau}\right)^2 + r^2\left(\frac{d\theta}{d\tau}\right)^2 + r^2\sin\theta^2\left(\frac{d\phi}{d\tau}\right)^2\right) \quad (12)$$

Here, τ is an affine parameter along the geodesics. Since the black hole have two Killing vectors ∂_t and ∂_ϕ, there are two constants of motion which can be labeled as E and L. They are given by,

$$g(r)\dot{t} = E \quad (13)$$

$$r^2\sin^2\theta\dot{\phi} = L \quad (14)$$

We choose $\theta = \pi/2$ and $\dot{\theta} = 0$ as the initial conditions. Hence $\ddot{\theta} = 0$. θ will remain at $\pi/2$ and the geodesics will be described in an invariant plane at $\theta = \pi/2$. With $\dot{t}$ and $\dot{\phi}$ given by Eqs. (13) and (14), the Lagrangian in Eq. (12) simplifies to be,

$$\dot{r}^2 + g(r)\left(\frac{L^2}{r^2} + h\right) = E^2 \quad (15)$$

Here, $2\mathcal{L} = h$. $h = 1$ corresponds to time-like geodesics and $h = 0$ corresponds to null geodesics. For a time-like geodesic, τ may be identified with proper time of the particle describing the geodesic. Comparing Eq. (15) with $\dot{r}^2 + V_{\text{eff}} = E^2$, one get the effective potential,

$$V_{\text{eff}} = \left(\frac{L^2}{r^2} + h\right)g(r) \quad (16)$$

By eliminating the parameter τ from the Eqs. (13) and (14), one can get a relation between ϕ and r as follows;

$$\frac{d\phi}{dr} = \frac{L}{r^2}\frac{1}{\sqrt{(E^2 - V_{\text{eff}})}} \quad (17)$$

In this paper, we will only focus on null geodesics. Hence $h = 0$ and the effective potential corresponds to,

$$V_{\text{eff}} = L^2\frac{g(r)}{r^2} \quad (18)$$

4 Radial null geodesics

The radial geodesics corresponds to the motion of particles with zero angular momentum ($L = 0$). Hence for radial null geodesics, the effective potential,

$$V_{\text{eff}} = 0 \tag{19}$$

The two equations for $\dot{t}$ and $\dot{r}$ simplifies to,

$$\dot{r} = \pm E; \qquad \dot{t} = \frac{E}{g(r)} \tag{20}$$

The above two equations lead to,

$$\frac{dt}{dr} = \pm\frac{1}{g(r)} = \pm\frac{1}{\left(1 - \frac{2M}{r} - cr\right)} \tag{21}$$

The above equation can be integrated to give the coordinate time t as a function of r as,

$$t = \pm\left(\frac{-2}{\sqrt{1-8cM}}\text{Tan}h^{-1}\left(\frac{-1+2cr}{\sqrt{1-8Mc}}\right) + \text{Log}\left(r - 2M - cr^2\right)\right) + \text{const}_{\pm} \tag{22}$$

The constant of integration is imaginary. However, when one compute the time t, the overall expression will be real. On the other hand, the proper time can be obtained by integrating,

$$\frac{d\tau}{dr} = \pm\frac{1}{E} \tag{23}$$

which leads to,

$$\tau = \pm\frac{r}{E} + \text{const}_{\pm} \tag{24}$$

When $r \to r_{\text{in}}$, $t \to \infty$. When $r \to r_{\text{in}}$, $\tau \to \frac{r_{\text{in}}}{E}$, which is finite. Hence the proper time is finite while the coordinate time is infinite. This is the same result one would obtain for the Schwarzschild black hole [22]. Figure 3 represents both times to show this. Note that we have picked the plus sign in this case, since we are studying the ingoing light rays.

5 Null geodesics with angular momentum ($L \neq 0$)

In this section, we will study the null geodesics with angular momentum.

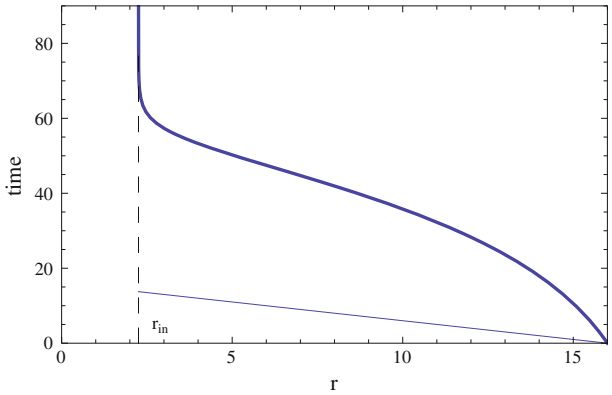

Fig. 3 The graph shows the relation of the coordinate time t and the proper time τ with the radius r. Here, $M = 1, c = 0.05$. The initial position is at $r = 16$. The inner horizon is at $r_{\text{in}} = 2.254$ and the outer horizon $r_{\text{out}} = 17.746$. The *dark curve* is for t and the *light curve* is for τ

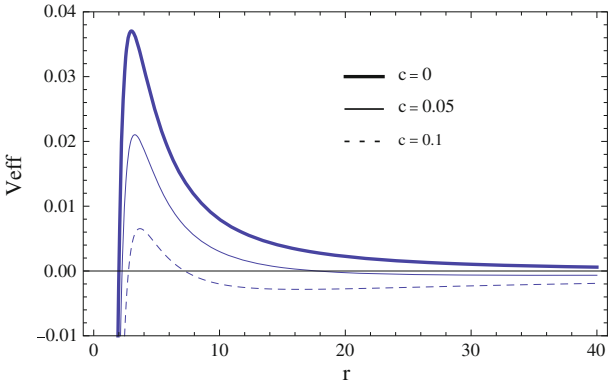

Fig. 4 The graph shows the relation of V_{eff} with the parameter c. Here, $M = 1$ and $L = 1$

5.1 Effective potential

In this case,

$$V_{\text{eff}} = g(r)\frac{L^2}{r^2} \tag{25}$$

For $r = r_{\text{in}}$ and r_{out}, $V_{\text{eff}} = 0$. In Fig. 4, the V_{eff} is given for various values of c. The potential for the Schwarzschild black hole is higher than for the black hole surrounded with the quintessence.

When the V_{eff} is expanded, it looks like,

$$V_{\text{eff}} = \frac{L^2}{r^2} - \frac{2L^2M}{r^3} - \frac{L^2c}{r} \tag{26}$$

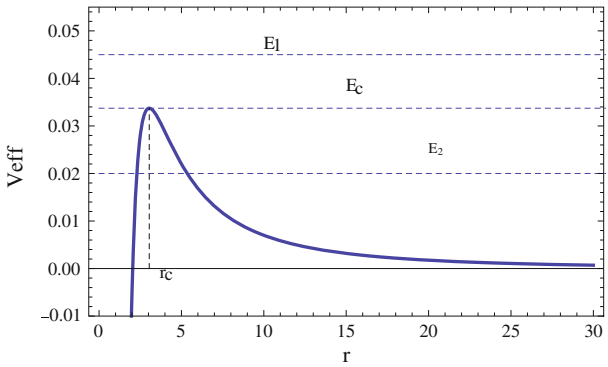

Fig. 5 The graph shows the relation of V_{eff} with the energy E. Here, $M = 1$, $c = 0.01$ and $L = 1$

The contribution to the effective potential from the quintessence is $-\frac{L^2 c}{r}$ compared to the Schwarzschild black hole. Note that in the Shwarzschild-de-Sitter case, the contribution is a constant $-L^2\Lambda$.

Since the energy and the effective potential are related by $\dot{r}^2 + V_{\text{eff}} = E^2$, the motion of the particles depend on the energy levels. In Fig. 5, the effective potential is plotted and three energy levels, E_1, E_c and E_2 are given. There are three different scenarios of motion of the particles as described below.

Case 1: $E = E_c$.

Here, $E^2 - V_{\text{eff}} = 0$ and $\dot{r} = 0$. The orbits are circular. Due to the nature of the potential at $r = r_c$, these are unstable. More details of the circular orbits will follow in the Sect. 5.2.

Case 2: $E = E_2$.

Here, $E^2 - V_{\text{eff}} \geq 0$ in two regions as is clear from Fig. 5. If the photons start the motion at $r > r_c$, it will fall to a minimum radius and fly back to large values of r. If the photons start the motion at $r < r_c$, then the photons will fall into the singularity crossing the inner horizon at $r = r_{\text{in}}$.

Case 3: $E = E_1$.

Here, $E^2 - V_{\text{eff}} > 0$ and $\dot{r} > 0$ for all r values. Hence the photons coming from large r values will cross the horizon at $r = r_{\text{in}}$ and will fall into the singularity.

5.2 Circular orbits

Circular orbits occurs when $E = E_c$ as explained in Sect. 5.1. Hence at $r = r_c$,

$$\dot{r} = 0 \Rightarrow V_{\text{eff}} = E_c^2 \tag{27}$$

and

$$\frac{dV_{\text{eff}}}{dr} = 0 \tag{28}$$

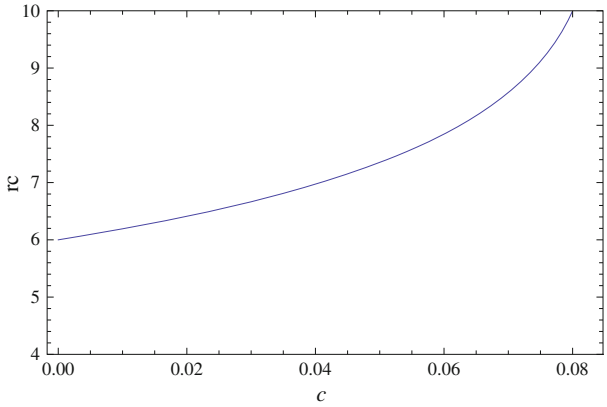

Fig. 6 The graph shows the relation of r_c with c. Here $M = 2$

From Eq. (28), one get two solutions for circular orbit radius r as,

$$r_{\pm} = \frac{1}{c}\left(1 \pm \sqrt{1 - 6cM}\right) \tag{29}$$

The larger root r_+ is greater than r_{out} and $r_{\text{in}} < r_- < r_{\text{out}}$. Since the motion of interest is between the horizons, the radius of circular orbits considered will be r_-. We will name it as r_c in the rest of the paper. Hence,

$$r_c = \frac{1}{c}\left(1 - \sqrt{1 - 6cM}\right) \tag{30}$$

In the Fig. 6, the radius of circular orbits are given as a function of c. One can observe that, the radius is bigger for non-zero values of c.

Due to the nature of the potential at $r = r_c$, the circular orbits at $r = r_c$ are unstable. The hypersurface at $r = r_c$ is known as the "photon sphere". For a detailed discussion about photon spheres see the paper by Claudel et.al [23]. When $c \to 0$, $r_c \to 3M$ which is the radius of the unstable circular orbit of the Schwarzschild black hole [22]. Circular orbits takes a special place in the studies of geodesics. The null circular orbit is the boundary between two qualitatively different regions. An interesting paper on null circular orbits of a hairy black hole is given by Hod [24].

The radius of the circular orbit r_c in Eq. (30) is independent of E and L. However, they are related to each other from Eq. (27) as,

$$\frac{E_c^2}{L_c^2} = \frac{g(r_c)}{r_c^2} = \frac{(r_c - 2M - cr_c^2)}{r_c^3} = \frac{1}{D_c^2} \tag{31}$$

Here, D_c is the impact parameter at the critical stage. When $c \to 0$, $D_c^2 \to 27M^2$ which is the impact parameter for the unstable circular orbits of the Schwarzschild black hole [22].

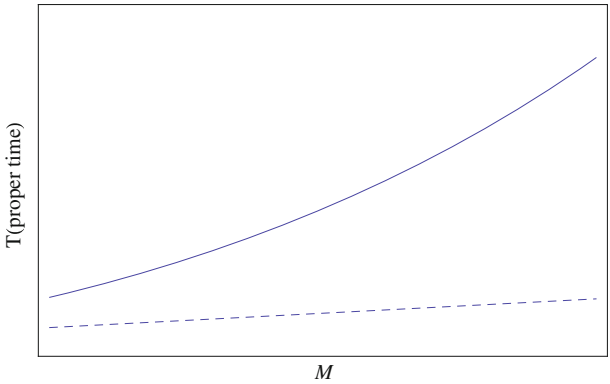

Fig. 7 The graph shows the relation of T_τ with the mass M. The *dark curve* is for $T_{\tau,\text{quintessence}}$ and the *dashed curve* is for $T_{\tau,\text{Sch}}$. Here, $c = 0.05$ and $L = 1$

5.2.1 The time period

The time period for the circular orbits for proper time (τ) as well as coordinate time (t) can be calculated with $\phi = 2\pi$. From Eq. (14),

$$T_\tau = \frac{2\pi r_c^2}{L} \tag{32}$$

The values T_τ for the Schwarzschild black hole is given by,

$$T_{\tau,Sh} = \frac{2\pi(3M)^2}{L} \tag{33}$$

Since the radius r_c is smaller for the Schwarzschild black hole, obviously T_τ is smaller for the Schwarzschild black hole.

From combining the two equations Eqs. (13) and (31),

$$T_t = \frac{2\pi r_c}{\sqrt{f(r_c)}} = \frac{2\pi r_c^{3/2}}{\sqrt{r_c - 2M - cr_c^2}} \tag{34}$$

The value for T_t for the Schwarzschild black hole is given by,

$$T_{t,Sh} = 3\sqrt{3}M \tag{35}$$

The graphs for the time periods are given in Figs. 7 and 8. By observing the graphs of the time periods, it is clear that the periods for the Schwarzschild black hole is smaller in comparison with the quintessence black hole. In a recent paper, Hod made an interesting observation that the null circular geodesics provide the shortest possible orbital period to circle a black hole [25].

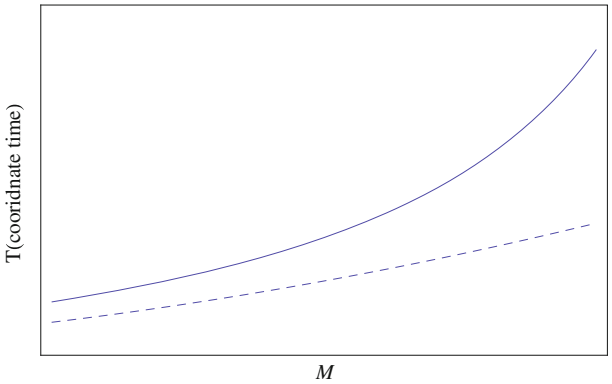

Fig. 8 The graph shows the relation of T_t with M. The *dark curve* is for $T_{t,\text{quintessence}}$ and the *dashed curve* is for $T_{t,\text{Sch}}$. Here $c = 0.01$ and $L = 1$

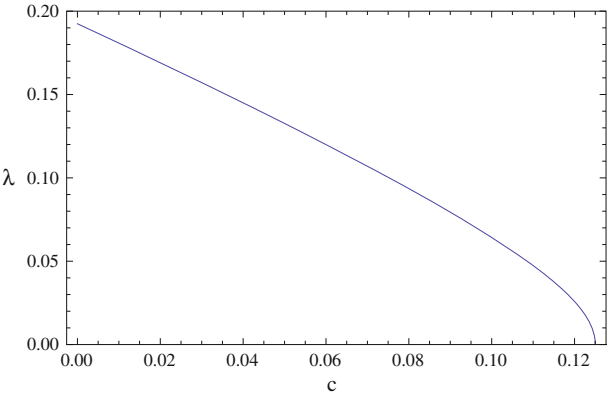

Fig. 9 The graph shows the Lyapunov exponent λ as a function of c. Here, $M = 1$

5.2.2 Lyapunov exponent for the unstable circular orbits

The instability time-scale of the unstable circular null geodesics is given by the Lyapunov exponent λ. The expression for λ was derived by Cardoso et al. [26] as (Fig. 9),

$$\lambda = \sqrt{\frac{-V''_{\text{eff}}(r_c)}{2\dot{t}(r_c)^2}} = \sqrt{\frac{-V''_{\text{eff}}(r_c) r_c^2 g(r_c)}{2L^2}}$$
$$= \sqrt{-c^2 - \frac{24M^2}{r^4} + \frac{18M}{r^3} - \frac{3}{r^2} - \frac{14cM}{r^2} + \frac{4c}{r}} \tag{36}$$

The instability of the circular orbits are more for the Schwarzschild black hole in comparison with the black hole with a non-zero c. In the paper by Cardoso et.al [26],

a critical exponent for instability of orbits were defined as,

$$\gamma = \frac{T_\lambda}{T_\tau} \tag{37}$$

Here, T_λ is the instability time scale which is related to the Lyapunov exponent as $T_\lambda = 1/\lambda$. Hence for large c values, λ becomes smaller for the same critical exponent.

5.3 Force on the photons

Since we have already computed the effective potential, one can obtain the effective force on the photon as,

$$F = -\frac{1}{2}\frac{dV_{\text{eff}}}{dr} = -\frac{3ML^2}{r^4} + \frac{L^2}{r^3} - \frac{cL^2}{2r^2} \tag{38}$$

Here, we have divided $\frac{dV_{\text{eff}}}{dr}$ by 2 since the equation of motion is written as $\dot{r}^2 + V_{\text{eff}} = E^2$. The first term, which is the Newtonian term, is attractive since it is negative. The second term is repulsive. The third term which is the force due to the quintessence matter, is attractive. It is interesting to notice that even though dark energy in cosmology is associated with a repulsive force to facilitate acceleration, in this situation, the dark energy term is attractive. This is a result due to the fact that we are studying a static configuration between the two horizons.

From Fig. 10, the force $F = 0$ at,

$$r_\pm = \frac{1}{c}\left(1 \pm \sqrt{1 - 6cM}\right) \tag{39}$$

One can see from the graph that $r_{\text{out}} < \frac{1}{c}\left(1 + \sqrt{1 - 6cM}\right)$. Since we are only concern about the motion for $r < r_{\text{out}}$, one can conclude that the force is positive for $r_c < r < r_{\text{out}}$ which leads to a repulsive force. On the other hand, for $r < r_c$, the force is negative leading to an attractive force.

The maximum repulsive force occur at $r = r_{\text{max}}$ where,

$$r_{\text{max}} = \frac{3}{2c}\left(1 - \sqrt{1 - \frac{16cM}{3}}\right) \tag{40}$$

6 Analysis of the geodesics with the variable $u = \frac{1}{r}$

Geodesics equation of motion can also be studied using a well known change of variable $u = \frac{1}{r}$. Then the Eq. (17) becomes,

$$\left(\frac{du}{d\phi}\right)^2 = f(u) \tag{41}$$

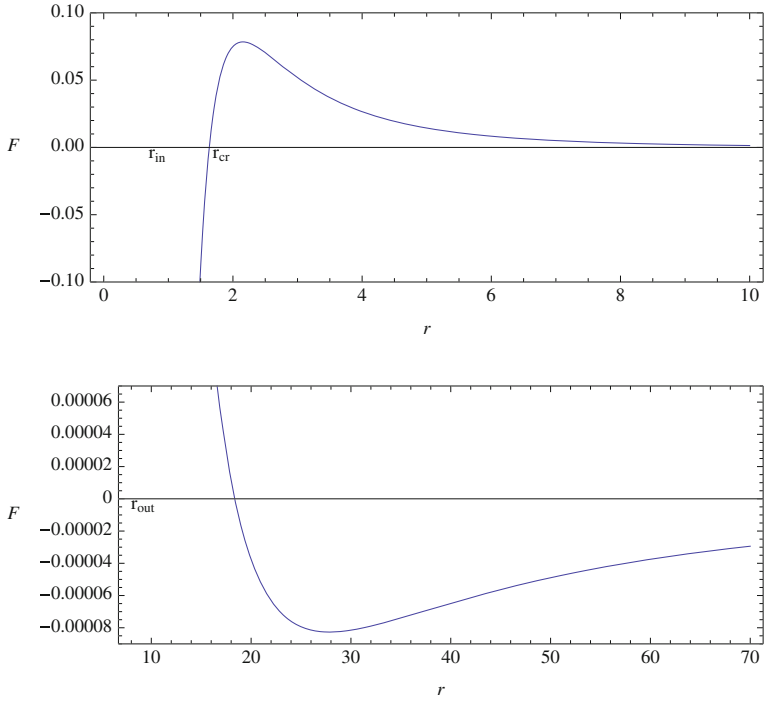

Fig. 10 The graphs shows the relation of F with r. Here $M = 0.5$, $c = 0.1$ and $L = 2$

where,

$$f(u) = 2Mu^3 - u^2 + cu + \frac{E^2}{L^2} \tag{42}$$

It is clear that the geometry of the geodesics depends on the nature of the roots of the equation $f(u) = 0$. Note that for any value of the parameters in the theory M, c, L, E, the function $f(u) \to -\infty$ for $u \to -\infty$ and $f(u) \to +\infty$ for $u \to +\infty$. Also, for $u = 0$, $f(u) = +\frac{E^2}{L^2}$. Therefore, $f(u)$ definitely has one negative real root (u_1). Let us name the roots of $f(u)$ as u_1, u_2 and u_3. The sum and the products of the roots u_1, u_2 and u_3 of the polynomial $f(u)$ are related to the coefficients of $f(u)$ as [27],

$$u_1 + u_2 + u_3 = \frac{1}{2M} \tag{43}$$

$$u_1 u_2 u_3 = -\frac{E^2}{2ML^2} \tag{44}$$

As discussed earlier, u_1 is real and negative. Therefore, the roots u_2, u_3 has to be positive if they are real. This conclusion comes from observing the signs of the Eqs. (43) and (44). Overall, the polynomial $f(u)$ has a negative (u_1) real root always. The other

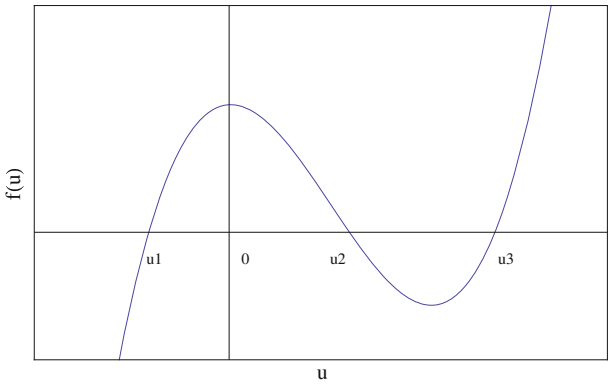

Fig. 11 The graph shows the function $f(u)$ for $M = 0.5$, $c = 0.01$, $L = 30$ and $E = 9$

two roots (u_2, u_3) will be either real or complex-conjugate. If they are real, then they will be positive. Also, if they are real, they could be degenerate roots as well.

The function $f(u)$ for general values of M, c, E and L is given in Fig. 11.

6.1 General solution for the geodesics in terms of u

From Eq. (40) derived above,

$$\left(\frac{du}{d\phi}\right) = \pm\sqrt{f(u)} \tag{45}$$

where $f(u)$ can be written as,

$$f(u) = 2M(u - u_1)(u - u_2)(u - u_3) \tag{46}$$

The "+" sign will be chosen without lose of generality. One can integrate the equation, $\frac{du}{\sqrt{f(u)}} = d\phi$ to get a relation between u and ϕ in terms of Jacobi-elliptic integral $\mathcal{F}(\xi, y)$ as,

$$\phi = \frac{-2\mathcal{F}(\xi, y)}{\sqrt{2m(u_2 - u_1)}} + \text{constant} \tag{47}$$

Here,

$$\sin\xi = \sqrt{\frac{(u_2 - u_1)}{(u - u_1)}} \tag{48}$$

$$y = \frac{(u_3 - u_1)}{(u_2 - u_1)} \tag{49}$$

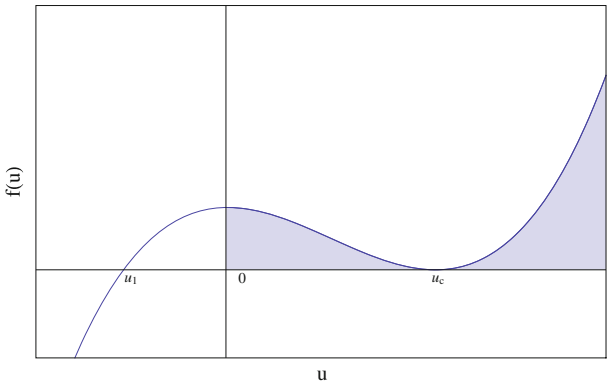

Fig. 12 The function $f(u)$ when it has degenerate roots leading to circular orbits. The *shaded area* represents the possible regions of motion. Here, $M = 0.5$, $c = 0.01$ and $r_c = 1.51142$

Depending on the values of the E, L, c, M, the integration constant would be real or imaginary. Also, u_1 is always real while the nature of u_2 and u_3 depend on the values of E, L, c, M.

6.2 Circular orbits

We will analyze in more ddetail the circular orbits here. In this case, the function $f(u)$ has a degenerate root at $u = u_c$. Hence, $f(u)$ can be written as,

$$f(u) = 2M(u - u_c)^2(u - u_1) \tag{50}$$

Here, $u_c = \frac{1}{r_c}$, where r_c is given by Eq. (30). From Eq. (42),

$$u_1 = \frac{1}{2M} - 2u_c \tag{51}$$

A null geodesic arriving from $r = r_s > r_c$ (or $u = u_s < u_c$) undergo unstable circular orbits at $r = r_c$ (or $u = u_c$). The form of the function $f(u)$ in this case is given in Fig. 12.

One can integrate the equation, $\frac{du}{\sqrt{f(u)}} = d\phi$ to get a relation between u and ϕ as,

$$u = u_1 + (u_c - u_1)tanh^2\left(\frac{\phi - \phi_0}{a_0}\right) \tag{52}$$

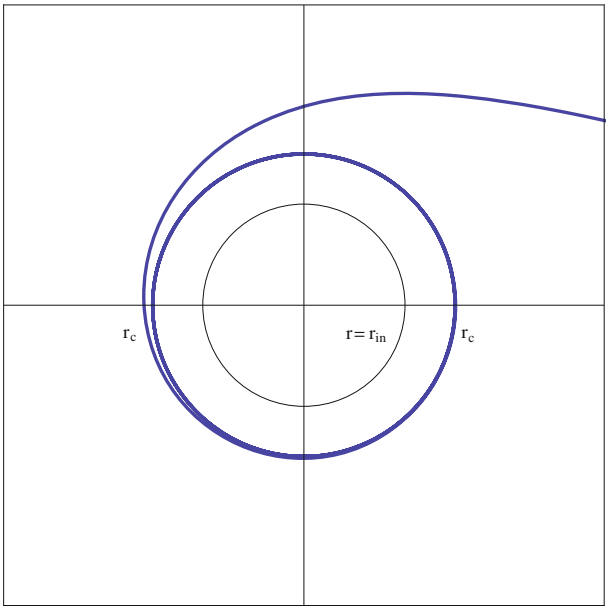

Fig. 13 The polar plot shows the critical null geodesics approaching the black hole from $r_s > r_c$. The geodesics have an unstable circular orbit at $r = r_c$. Here, $M = 0.5$, $c = 0.01$ and $r_c = 1.51142$

ϕ_0 and a_0 are given by,

$$\phi_0 = a_0 tanh^{-1}\left(\sqrt{\frac{u_1 - u_s}{u_1 - u_c}}\right) \tag{53}$$

$$a_0 = -\sqrt{\frac{2}{M(u_c - u_1)}} \tag{54}$$

In Fig. 13, the polar plot of the null geodesics are given for photons arriving from $r_s > r_c$ and having an unstable circular orbit at $r = r_c$.

6.3 Unbounded orbits

Case 2 : $\mathbf{E = E_2}$

Here, we will study Case 2 given in the Sect. 5.1. In this case, $f(u) = 0$ has three real roots. Therefore, the motion is possible in two regions given as 1 and 2 in Fig. 14.

If the particle starts far from the black hole at $r = r_s$, it will fall until $r = r_2 = 1/u_2$ and fly away from the black hole. The equation of motion is the same as given in Eq. (46). The integration constant is chosen such that $\phi = 0$ for $r = r_s$. The corresponding motion is given in Fig. 15.

The second possibility for $E = E_2$ corresponds to the motion starting from $r = r_3$ (or $u = u_3$). Here, $r_3 < r_c$. Hence the particle will fall into the singularity crossing the horizon at $r = r_{\text{in}}$. In this case, the solutions for ϕ is similar as in Eq. (47). Therefore,

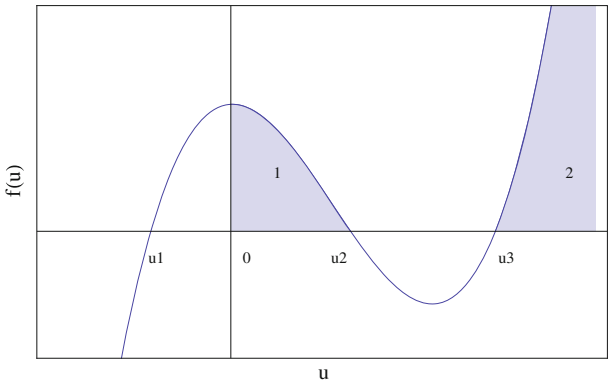

Fig. 14 The graph shows the function $f(u)$ when it has three real roots. Here $M = 0.5$, $c = 0.01$, $L = 30$ and $E = 9$

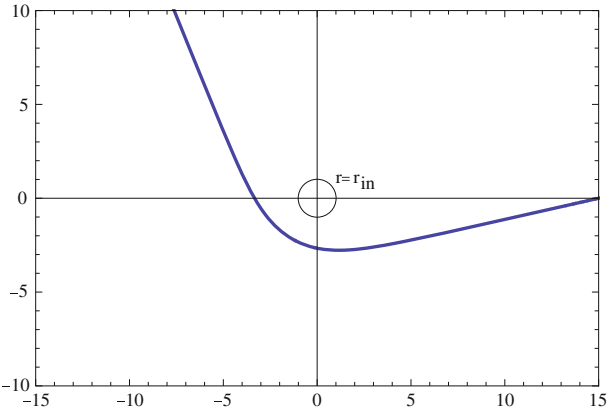

Fig. 15 The polar plot shows the null geodesics approaching the black hole from $r = r_s$. Here, $M = 1$, $c = 0.01$, $L = 30$, $E = 9$, $r_s = 15$ and $r_2 = 2.54082$. The inner horizon is at $r_{\text{in}} = 1.01021$

we will omit the explicit expressions for the ϕ in this case. The integration constant is chosen such that $\phi = 0$ when $u = u_3$. The corresponding motion is given in Fig. 16.

Case 3 : E = E$_1$

Here, we will study the Case 3 given in the Sect. 5.1. In this case, $f(u) = 0$ has only one real root as given in Fig. 17.

The motion is possible in the shaded area. For all values of r, the photons will fall into the black hole. The equation of motion is same as in Eq. (47). However, in this case, u_2 and u_3 are both imaginary and u_1 is real. The corresponding motion is given in Fig. 18.

7 Application of null geodesics: gravitational lensing by the quintessence black hole

Bending of light and gravitational lensing is an important aspect one can study related to null geodesics around black holes. The unbounded orbit with energy $E = E_2$

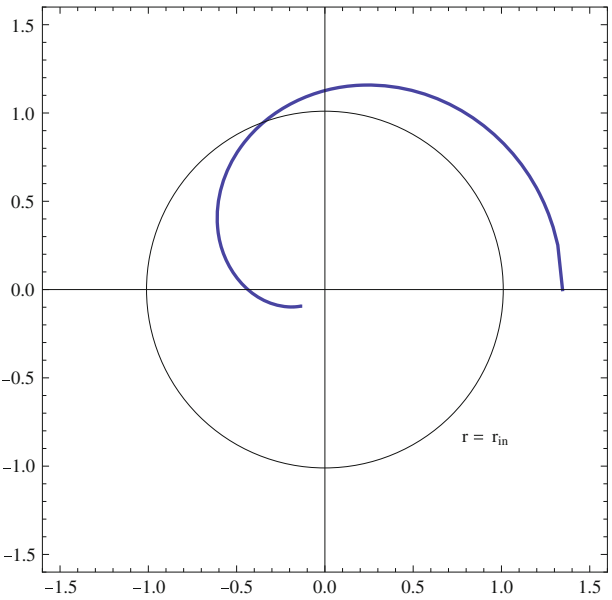

Fig. 16 The polar plot shows the null geodesics falling into the black hole from $r = r_3$. Here, $M = 1$, $c = 0.01$, $L = 30$, $E = 11$, $r_3 = 1.34587$ and $r_{\text{in}} = 1.01021$

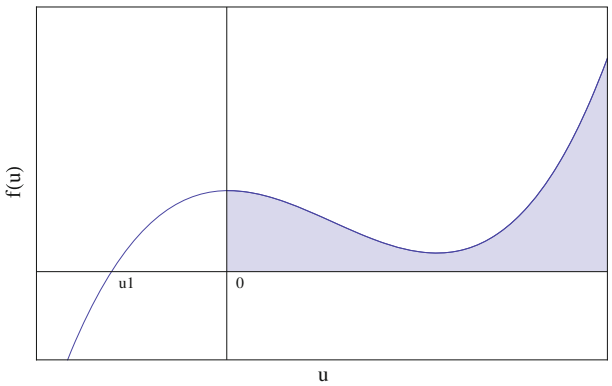

Fig. 17 The graph shows the function $f(u)$ when it has only one real root. Here, $M = 0.5$, $c = 0.01$, $L = 21$, $E = 9$ and $u_1 = -0.363391$

studied in Sect. 6.3 clearly represents how photons deviate from its original path when moving around a black hole. The motion is given in Fig. 15.

7.1 Closest approach r_o

To study the bending of light, let us first calculate the closest approach distance r_o for the photon with energy E_2. It is defined by the value of r when $\frac{dr}{d\phi} = 0$. From

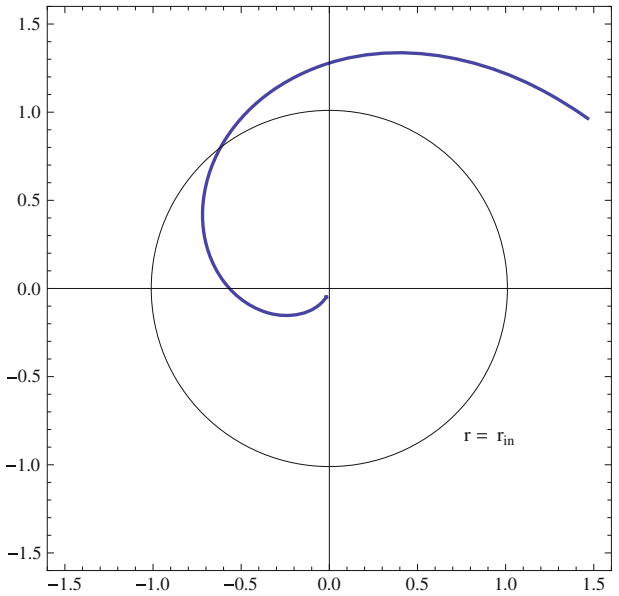

Fig. 18 The polar plot shows the null geodesics approaching the black hole from $r = 15$. Here, $M = 0.5$, $c = 0.01$, $L = 21$ and $E = 9$

Eqs. (41) and (42),

$$\left(\frac{1}{r^2}\frac{dr}{d\phi}\right)^2 = f(r) = \frac{2M}{r^3} - \frac{1}{r^2} + \frac{c}{r} + \frac{E^2}{L^2} \tag{55}$$

$\frac{dr}{d\phi} = 0$ corresponds to the roots of $f(r) = 0$ which also could be written as,

$$r^3 + D^2cr^2 - D^2r + 2MD^2 = 0 \tag{56}$$

From Fig. 13, the roots of the above equation corresponds to r_1, r_2, r_3 which are the inverse of u_1, u_2, u_3. Since $r_1 < 0$, the roots to be considered are r_2 or r_3. From Fig. 5, r_2 and r_3 are the positions where $E_2 = V_{\text{eff}}$. Clearly, $r_3 < r_2$ (since $u_3 > u_2$). Also, $r_3 < r_c < r_2$. Hence, the root we will choose for the closest approach is r_2.

Now, one can use the well known techniques in determining the roots of a cubic polynomial to obtain r_0 from Eq. (55) as,

$$r_o^{\text{quintessence}} = 2\sqrt{-\frac{p}{3}}\cos\left(\frac{1}{3}\cos^{-1}\left(\frac{3q}{2p}\sqrt{-\frac{3}{p}}\right)\right) - \frac{D^2c}{3} \tag{57}$$

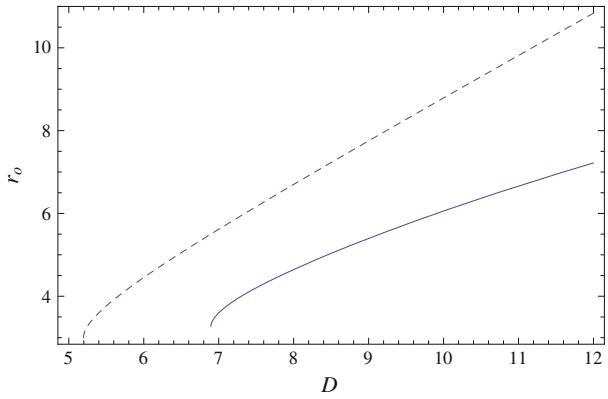

Fig. 19 The graph shows the closest approach r_o for the quintessence black hole (*dark curve*) and the Schwarzschild black hole (*dashed curve*) as a function of the impact parameter D. Here, $M = 1$ and $c = 0.05$. $D_c = 6.8956$ for the quintessence black hole and $D_c = 5.19615$ for the Schwarzschild black hole

Here, p and q are given by,

$$p = -\frac{(D^4c^2 + 3D^2)}{3} \tag{58}$$

$$q = \frac{54MD^2 + 9cD^4 + 2D^6c^3}{27} \tag{59}$$

When $c \to 0$, r_o approaches the well known value for the Schwarzschild black hole given by [28],

$$r_o^{\text{Sch}} = \frac{2D}{\sqrt{3}} \cos\left(\frac{1}{3}\cos^{-1}\left(\frac{-\sqrt{27}M}{D}\right)\right) \tag{60}$$

Figure 19 shows the closest approach for the quintessence black hole and the Schwarzschild black hole.

7.2 Bending angle

Now, we will compute the angle of deflection of light for the quintessence black hole. In a paper by Amore et.al. [29], a new method was introduced to compute the deflection angle for a static spherically symmetric space-time. This method yields highly accurate analytical results. In the paper, they applied the technique to well known metrics. One of them was the metric in Weyl gravity [30,31]. In Weyl gravity, the metric is given by,

$$ds^2 = -g(r)dt^2 + g(r)^{-1}dr^2 + r^2(d\theta^2 + \sin^2\theta d\phi^2) \tag{61}$$

$$g(r) = 1 - \frac{2\beta}{r} + \gamma r - kr^2 \tag{62}$$

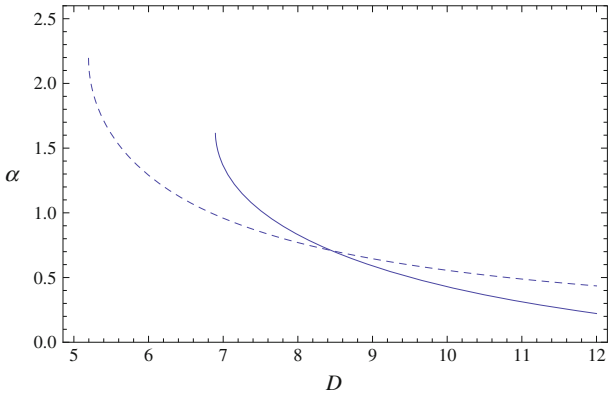

Fig. 20 The graph shows the bending angle α for the quintessence black hole (*dark curve*) and the Schwarzschild black hole (*dashed curve*) as a function of the impact parameter D. Here, $M = 1$ and $c = 0.05$. $D_c = 6.8956$ for the quintessence black hole and $D_c = 5.19615$ for the Schwarzschild black hole

Even though the context in which the Weyl gravity and the quintessence black hole are formulated are different, one can see that for $k = 0$ and $\gamma = -c$, the Weyl gravity geometry and the quintessence black hole geometry is the same!. Therefore, the bending angle obtained by Amore et.al [29] for the Weyl gravity can be modified to obtain the angle for the quintessence black hole as,

$$\alpha_{\text{quintessence}} = \frac{4M}{r_o} + \frac{4M^2}{r_o^2}\left(\frac{15\pi}{16} - 1\right) + c\left(r_o - M + \frac{3\pi M}{2}\right) + c^2\frac{r_o^2}{2} \tag{63}$$

Note that here, r_o is the one given in Eq. (56) for the quintessence black hole.

When $c \to 0$, one obtain the well known bending angle for the Schwarzschild black hole, as,

$$\alpha_{\text{Sch}} = \frac{4M}{r_o} + \frac{4M^2}{r_o^2}\left(\frac{15\pi}{16} - 1\right) \tag{64}$$

Here, r_o corresponds to the one given in Eq. (60). We will substitute the respective expressions for r_0 in terms of the impact parameter D for both black holes and plot the deflection angle as a function of the impact parameter D.

From Fig. 20, the photons with the same impact parameter bends more around the quintessence black hole for small D and less for large D. We like to mention here that Liu et.al [32] did studied the gravitational frequency shift and deflection of light for the black holes surrounded by the quintessence for various values of the state parameter ω_q. There, the function u was computed as a first order approximation where as here the exact solution is used.

8 Conclusion

We have studied the null geodesics of a black hole surrounded by dark energy. Here, we have chosen quintessence as the candidate for dark energy and the black hole solution studied was derived by Kiselev [15]. The equations for the geodesics were solved exactly for various values of energy and angular momentum of the photons. All possible motions are presented. The circular orbits are studied in detail and are shown to be unstable. We have also computed the Lyapunov exponent λ which gives the instability time scale for the unstable geodesics. It is shown that λ is smaller for the dark energy black hole in comparison with the λ for the unstable circular orbits for the Schwarzschild black hole.

As an application of the photon motion studied here, we have studied the light deflection for this particular black hole and have done comparisons with the Schwarzschild black hole. The photons with the same impact parameter bends more around the quintessence black hole for small D and less for large D.

As an extension of this work, one could study the motion of particles around the charged version of the quintessence black hole.

Acknowledgments This work was supported in part by the Faculty Summer Fellowship (2010) of Northern Kentucky University.

References

1. Perlmutter, S. et al.: Measurements of Ω and Λ from 42 high-redshift supernovae. Astrophys. J. **517**, 565 (1999)
2. Riess, A.G. et al.: Observational evidence from supernovae for an accelerating universe and a cosmological constant. Astron. J. **116**, 1009 (1998)
3. Riess, A.G. et al.: BVRI light curves for 22 Type Ia supernovae. Astron. J. **117**, 707 (1999)
4. Spergel, D.N. et al.: (WMAP collaboration), *Wilkinson microwave anisotropy probe (WMAP) three ear results: implications for cosmology*. Astrophys. J. Suppl **170**, 377 (2007)
5. Tegmark, M. et al.: (SDSS collaboration) *cosmological parameters from SDSS and WMAP*. Phys. Rev. D **69**, 103501 (2004)
6. Seljak, U. et al.: Cosmological parameter analysis including SDSS Lyα forest and galaxy bias: constraints on the primordial spectrum of fluctuations, neutrino mass, and dark energy. Phys. Rev. D **71**, 103515 (2005)
7. Copeland, E.J., Sami, M., Tsujikawa, S.: Dynamics of dark energy. Int. J. Modern. Phys. D **15**, 1753 (2006)
8. Weinberg, S.: Rev. Mod. Phys. **61**, 1 (1989)
9. Carroll, S.M.: Quintessence and the rest of the world: suppressing long-range interactions. Phys. Rev. Lett. **81**, 3067 (1998)
10. Khoury, J., Weltman, A.: Chameleon fields: awaiting surprises for tests of gravity in space. Phys. Rev. Lett. **93**, 171104 (2004)
11. Armendariz-Picon, C., Mukhanov, V., Steinhardt, P.J.: Dynamical solution to the problem of a small cosmological constant and late-time cosmic acceleration. Phys. Rev. Lett. **85**, 4438 (2000)
12. Padmanabhan, T.: Accelerated expansion of the universe driven by tachyonic matter. Phys. Rev. D **66**, 021301 (2002)
13. Caldwell, R.R.: A phantom menace? Cosmological consequences of a dark energy component with super-negative equation of state. Phys. Lett. B **545**, 23 (2002)
14. Gasperini, M., Piassa, M., Veneziano, G.: Quintessence as a runaway dilaton. Phys. Rev. D **65**, 023508 (2002)
15. Kiselev, V.V.: Quintessence and black holes. Class. Quan. Grav. **20**, 1187 (2003)

16. Chen, S., Jing, J.: Quasinormal modes of a black hole surrounded by quintessence. Class. Quant. Grav. **22**, 4651 (2005)
17. Zhang, Y., Gui, Y., Yu, F.: Quasinormal modes of a Schwarzschild black hole surrounded by free static spherically symmetric quintessence: electromagnetic perturbations. Gen. Relativ. Gravit. **39**, 1003 (2007)
18. Zhang, Y., Gui, Y., Yu, F.: Dirac quasinormal modes of a Schwarzschild black hole surrounded by free static spherically symmetric quintessence. Chin. Phys. Lett. **26**, 030401 (2009)
19. Ma, C., Gui, Y., Wang, W., Wang, F.: Massive scalar field quasinormal modes of a Schwarzschild black hole surrounded by quintessence. Central Eur. J. Phys. **6**, 194 (2008)
20. Varghese, N., Kuriakose, V.C.: Quasinormal modes of Reissner-Nrdstrom black hole surrounded by quintessence. Gen. Relativ. Gravit. **41**, 1249 (2009)
21. Chen, S., Wang, B., Su, R.: Hawking radiation in a d-dimensional static spherically-symmetric black Hole surrounded by quintessence. Phys. Rev. D **77**, 124011 (2008)
22. Chandraseckar, S.: Mathematical Theory of Black Holes. Oxford Press, Oxford (1980)
23. Claudel, C.M., Virbhadra, K.S., Ellis, G.F.R.: The geometry of photon spheres. J. Math. Phys. **42**, 818 (2001)
24. Hod, S.: Hairy black holes and null circular geodesics. Phys. Rev. D **84**, 124030 (2011)
25. Hod, S.: The fastest way to circle a black hole. Phys. Rev. D **84**, 104024 (2011)
26. Cardoso, V., Miranda, A.S., Berti, E., Witeck, H., Zanchin, V.T.: Geodesics stability, Lyapunov exponents and quasinormal modes. Phys.Rev. D **79**, 064016 (2009)
27. Abramowitz, M., Stegun, A.: Handbook of Mathematical Functions. Dover, New York (1977)
28. Biressa, T., de Freitas Pacheco, J.A.: The cosmological constant and the gravitational light bending. Gen. Relativ. Gravit. **43**, 2649 (2011)
29. Amore, P., Arceo, S., Fernandez, F.M.: Analytical formulas for gravitational lensing: higher order calculation. Phys. Rev. D **74**, 083004 (2006)
30. Pireaux, S.: Light deflection in Weyl gravity: critical distances for photon paths. Class. Quantum. Grav. **21**, 1897 (2004)
31. Pireaux, S.: Light deflection in Weyl gravity: constraints on the linear parameter. Class. Quantum. Grav. **21**, 4317 (2004)
32. Liu, M., Lu, J., Gui, Y.: The influence of free quintessence on gravitational frequency shift and deflection of light with 4D momentum. Eur. Phys. J. C **59**, 107 (2009)